Progress In Electromagnetics Research B, Vol. 88, 175–195, 2020

Dual Feed Wideband Annular Ring Microstrip Antenna with Circular DGS for Reduced SAR

Mahesh Munde*, Anil Nandgaonkar, and Shankar Deosarkar

Abstract—In this article quad-band circular antenna is designed for multiband devices operated close to human body, and the investigation on parametric study for length of feed, width of feed, and length of ground is carried out. Specific absorption rate (SAR) is also evaluated and found to exceed standard limits for lower band. Further investigation to reduce the value of SAR leads to the design of an annular ring antenna with partial ground. Parametric study on the ratio of outer to inner ring radii is carried out to excite higher resonant modes and optimize the performance of annular ring antenna. SAR is evaluated for different bands, and 9% reduction is observed for same dimensions of circular antenna with partial ground, but SAR still exceeds the limit for lower band. A novel approach of using dual feeds with half operating input power in magnitude and 180° out phase at each port for SAR reduction and performance optimization is presented in this work. Annular ring antenna with parametric study on variation in the ratio of ring radii and circular defect in ground structure is performed, and it leads to wideband operation, gain enhancement, and reduction in SAR. SAR reduction achieved is in the range of 66.93% to 82.15% in 1-gram of tissue and 64.43% to 82.20% in 10-gram of tissue at different bands and well within the limits for all the operating bands.

1. INTRODUCTION

Antenna is one of the major devices in wireless communication, and the design of antenna has many challenges due to rapid technological changes. Calling Tablet uses multiband multisystem antennas. Multiband antennas can meet the demand for multisystem requirement. Fourth generation wireless standard operates from 400 MHz to 4 GHz. Higher frequencies from the band are allocated in Asia and Europe so as to provide larger bandwidths [1–3]. In annular ring antenna TM_{mn} is used as there is no field variations in Bessel's and Neuman's functions of order m. TM_{11} is dominant in these antennas, so to achieve multiband resonance higher modes must be excited, and the frequency of resonance of circular antenna is given by the following Equation (1) [4–6].

$$F_{mn} = \left(\frac{x_{mn}c}{2\pi r\sqrt{\varepsilon_{eff}}}\right) \tag{1}$$

where F_{mn} is the resonant frequency, x_{mn} the first order Bessel function root, c the speed of light in free space, r the radius of patch, and ε_{eff} the effective dielectric constant.

In a circular antenna, TM_{11} mode is dominant, and its resonant frequency is given by Equation (2). ε_{eff} is given by Equation (3); Equation (4) gives effective radius (r_e) after consideration of fringing fields; and Equation (5) gives the width of feed [6–8].

$$F_{mn} = \frac{1.8412C}{2\pi r_e\sqrt{\varepsilon_{eff}}} \tag{2}$$

Received 18 July 2020, Accepted 9 September 2020, Scheduled 1 October 2020

* Corresponding author: Mahesh Munde (maheshmunde79@gmail.com).

The authors are with the Electronics and Telecommunication Engineering Department, Dr. Babasaheb Ambedkar Technological University, Lonere, Maharashtra, India.

$$\varepsilon_{eff} = \left(\frac{\varepsilon_r + 1}{2}\right) + \left(\frac{\varepsilon_r - 1}{2}\right)\left(1 + \frac{12h}{w}\right)^{\frac{-1}{2}} \tag{3}$$

$$r_e = r\left(1 + \frac{2h}{\pi r \varepsilon_r}\left(\ln\left(\frac{\pi r}{2h}\right) + 1.7726\right)\right)^{\frac{1}{2}} \tag{4}$$

$$w_f = \frac{7.48h}{e^{\left(\frac{z_0\sqrt{\varepsilon_r+1.41}}{87}\right)}} - 1.25t \tag{5}$$

where ε_r is the relative permittivity, h the substrate height, w the width, z_0 the single ended impedance of microstrip feedline, and t the thickness of the stripline.

Defective Ground Structure (DGS) utilises defect in ground plane to enhance gain and bandwidth, and it is also useful to achieve multiband operation. DGS suppresses backward radiation and reduces cross-polarization levels. Various methods to enhance bandwidth and improve system capacity are proposed by using various symmetrical and asymmetrical defects in ground plane [9]. Microstrip patch antennas with single or multiple slots are employed to reduce mutual coupling and to suppress higher order harmonics. When a slot is introduced in ground plane, it modifies the current distribution in the ground and minimizes surface waves so that it acts as a band stop filter. Stopband characteristics at resonant frequency can be obtained by means of optimising the size of slot. Many models are proposed for equivalent circuits, and an ideal transformer method is simple, accurate, and can identify the location of DGS and is most suitable for slotted ground with a microstrip feedline. Different shapes of DGS have their own characteristics and accordingly create diverse performances [10–13].

Annular ring antenna is substantially smaller than its counterparts and reveals high input impedance, when it is operated in the fundamental mode. Also, the ratio of outer to inner radii regulates the separation among the modes and by a proper choice of the ratio of radii, bandwidth can be broadened [5]. In this article, a circular antenna is designed, and parametric study is carried out for the length of microstrip feed, width of feed, and size of slot in ground to obtain multiband operation and improve the performance of circular antenna, so that antenna can be used in portable devices (calling tablet), and SAR is evaluated and found to exceed limits issued by FCC and IEEE. An annular ring antenna is designed, and parametric study is carried out on the ratio of outer to inner radii so as to excite higher order modes of TM_{m1} and TM_{m2} for better radiation characteristics as mentioned in [5]. Also, SAR is evaluated and compared with annular ring antenna and is noticed to be reduced by 9% but still exceeds limits for lower band. To reduce SAR, a dual feed annular ring microstrip antenna with half input power at each port is designed, and rectangular partial ground is replaced with a circular slotted ground underneath annular patch. A circular DGS is chosen, and by means of parametric analysis on size of the slot, the performance can be easily optimised. DGS is utilised to achieve better impedance matching and wideband operation as a primary function, and secondarily it minimizes surface waves which reduces SAR.

2. ANALYSIS OF ANTENNA AND DGS

2.1. Design of Circular Antenna

The multiband antenna is designed using an FR-4 lossy substrate having dielectric constant (ε) 4.3, height 1.53 mm, and loss tangent (δ) 0.025. The circular antenna with a microstrip feedline having fundamental resonant mode TM_{11} is designed to cover lower fundamental band of 0.9 GHz. The effective radius calculated is 4.7 cm; substrate length considered is approximately 1.5 times of the diameter of circular patch (140 mm); and further, other parameters can be optimized using parametric study.

2.1.1. Parametric Study on Length of Feed (L_f)

The length of microstrip feedline is varied from 19 mm to 25 mm, and it is observed that there is a slight change in the reflection coefficient and resonant frequency which is depicted in Figure 1. Gain is constant for all the variations of feedline length. The performance of antenna is better when feed length is optimized to 23 mm as all the desired bands are covered.

2.1.2. Parametric Study on Width of Feed (W_f)

The length of feed is fixed to 23 mm, and W_f is varied from 2.8 mm to 4.4 mm. The optimum value for better impedance matching is obtained at the width of 3.6 mm which is depicted in Figure 2. Gain is constant for all the bands.

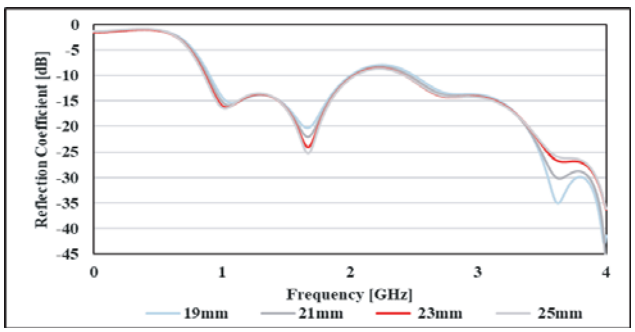

Figure 1. Reflection coefficient for different feed lengths.

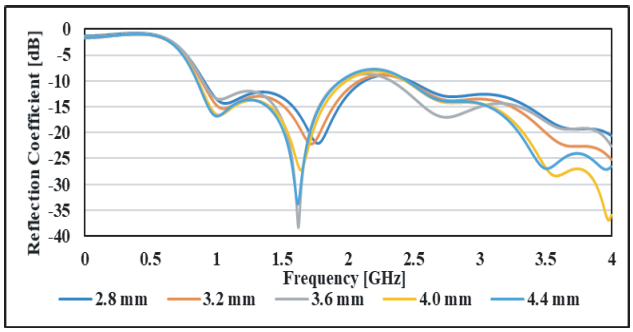

Figure 2. Reflection coefficient for different feed widths.

2.1.3. Parametric Study on Length of Ground (L_g)

Parametric study is carried out on L_g, and optimum performance of antenna is obtained when ground length (L_g) is 23 mm which is equal to the feed length and substrate size of $140 \times 140 \times 1.6\,\text{mm}^3$. Substrate width is optimized to 104 mm by observing gain and impedance variations. Figure 3 shows the designed circular antenna with full ground in top and bottom views respectively, and Figure 4 depicts the circular antenna with partial ground, and all dimensions are in mm.

Figure 5 shows reflection coefficient and variation in impedance for various values of L_g. Better impedance match and broadening of frequency bands on the curve are observed when the length of partial ground is 23 mm.

Performance parameters are discussed in this section, not only reflection coefficient but other parameters like gain, directivity, radiation pattern, VSWR, power accepted, power radiated, and losses

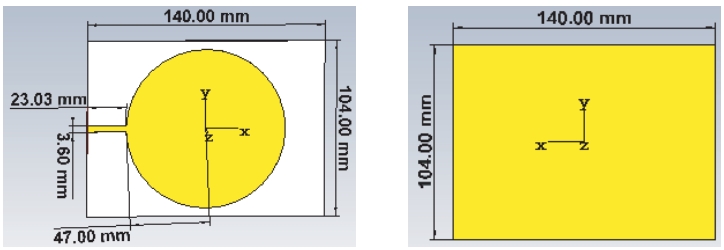

Figure 3. Top and bottom view of circular antenna with full ground.

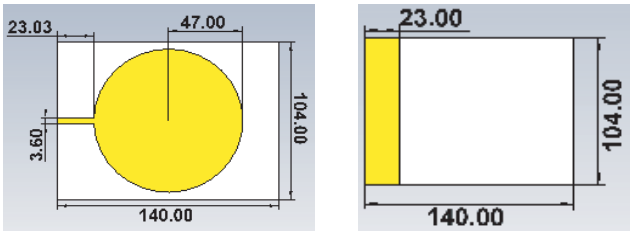

Figure 4. Top and bottom view of circular antenna with optimized partial ground.

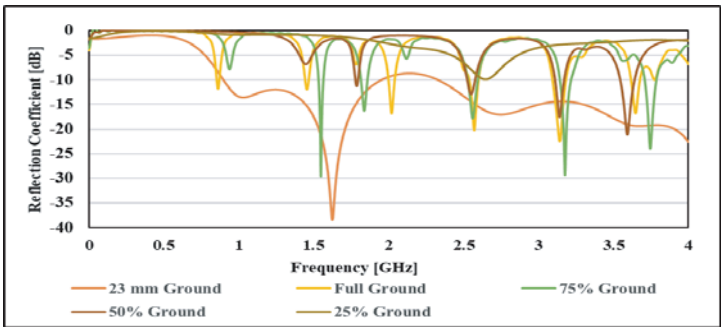

Figure 5. Reflection coefficient v/s frequency for different sizes of ground.

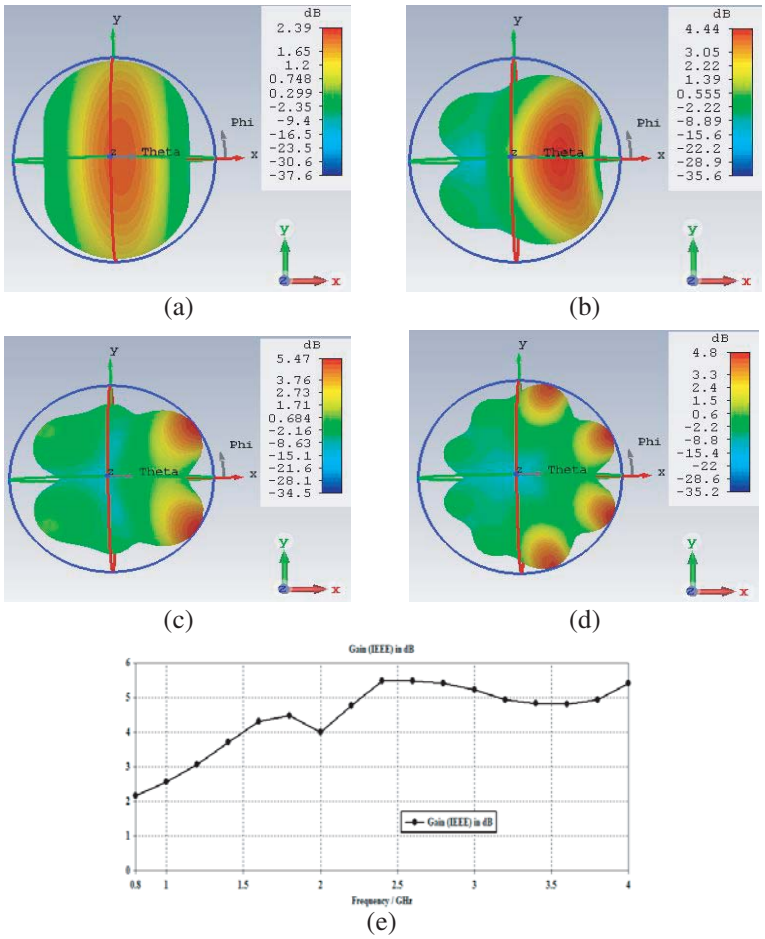

Figure 6. (a) to (d) Gain at desired frequencies, (e) gain v/s frequency over entire band.

in metal and dielectric also play a vital role in analysing the performance of antenna. Figures 6(a) to (d) depict 3-D gain in dB, and Figures 7(a) to (d) show 3-D directivity in dBi, at 0.9 GHz, 1.8 GHz, 2.4 GHz, and 3.5 GHz, respectively. Figure 6(e) shows the gain over entire frequency band for the circular antenna.

Figures 8(a), (b), and (c) show the radiation pattern in X-Z plane, Y-Z plane, and X-Y plane, respectively. Radiation pattern is donut-shaped at lower frequency and gets distorted due to sidelobes at higher frequencies. It is ideal for the fundamental frequency of 0.9 GHz in E-plane and H-plane. When higher modes are excited, it gets distorted, and some of the power is lost in sidelobes.

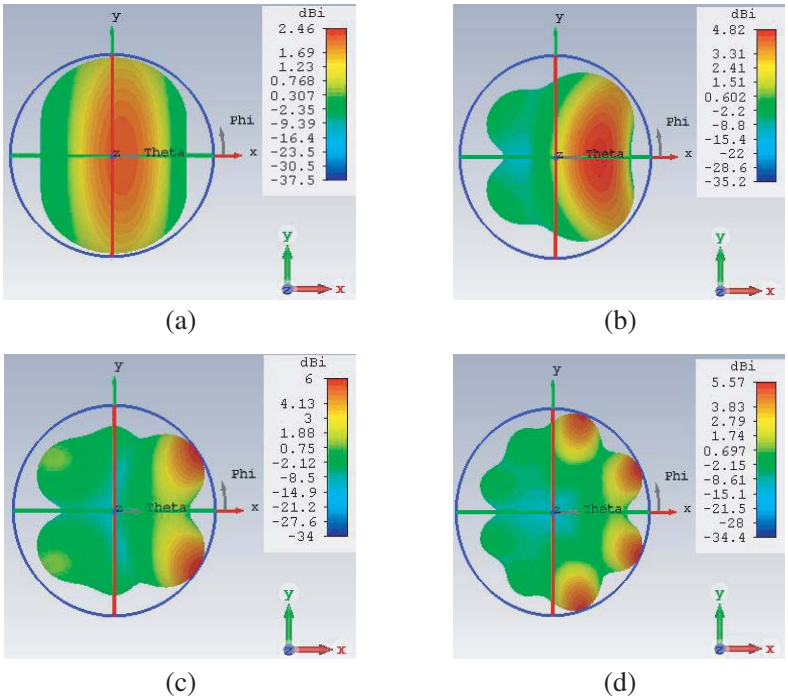

Figure 7. (a) to (d) Directivity in dBi at desired frequencies.

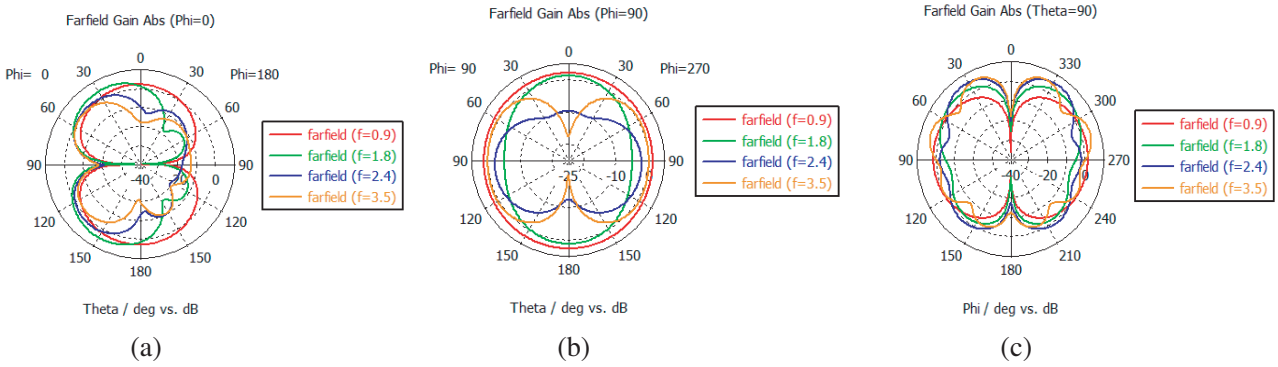

Figure 8. Simulated combined radiation pattern, (a) X-Z plane, (b) Y-Z plane, (c) X-Y plane.

Figure 9 depicts VSWR and is in the range $1 < \text{VSWR} < 2$ for the entire band from 0.9 GHz to 4 GHz excluding small range of frequency band in between 1.9825 GHz and 2.2956 GHz for the circular antenna.

Input power applied in simulation is 500 mW, for practical antenna it is necessary to calculate quality factor as it is a figure of merit which decides the losses in antenna. Losses in antenna are entirety of radiation loss, ohmic loss, surface loss, and dielectric loss. Surface loss is less than all other losses so is neglected during simulation. To achieve wide or broad bandwidth quality factor should be as low as possible. Figure 10 shows accepted power, radiated power, and losses, so the performance of antenna can be analysed easily from these curves, as ohmic loss and dielectric loss directly contribute to SAR.

Specific Absorption Rate (SAR) is a metric to quantify and record the localization of the amount of radiated power absorbed by the tissue and is derived from the electric field induced inside the tissue. It is a point quantity, and the value varies from one location to another location inside the tissue. The value of SAR depends upon three parameters, induced electric field, conductivity of tissue and density

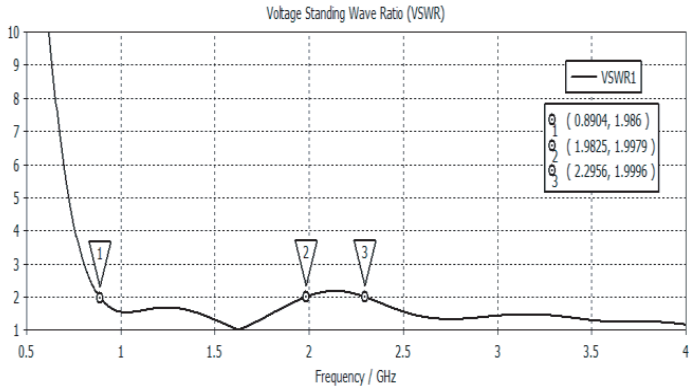

Figure 9. VSWR v/s frequency.

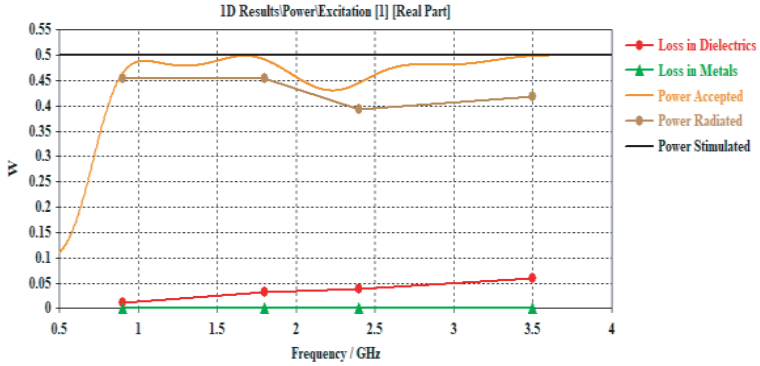

Figure 10. Input power and losses curve.

of tissue. SAR represents the time rate of microwave energy absorbed inside the human tissue and is represented by the following Equation (6) [14].

$$SAR = \frac{\sigma}{2\rho}\left(\frac{d}{dt}\left(E_t^2\right)\right) \tag{6}$$

where σ is the conductivity of tissue in S/m, ρ the density of tissue in kg/m^3, and E_t the internal induced electric field in V/m.

Specific Anthropomorphic Mannequin (SAM) phantom model which comprises shell and fluid is used for SAR evaluation for 1-gram tissue mass and is illustrated in Figures 11(a) to (d). Simulated results are exhibited for 10-gram tissue mass in Figures 12(a) to (d) at 0.9 GHz, 1.8 GHz, 2.4 GHz, and 3.5 GHz, respectively. Figure 13 shows the comparison of variation in simulated results when reflection coefficient of designed antenna is evaluated over 0–4 GHz band. The designed antenna is imported in the biomedical project where SAM phantom model is available in CST-MW studio tools and is aligned and placed at a distance of 10 mm from SAM phantom head model. In simulator 40 dB accuracy level in settings is adjusted, simulation run performed, and reflection coefficient evaluated. Figure 14 exhibits the variation in radiation pattern in the presence of SAM phantom model with above discussed settings. It is evident from Figure 13 reflection coefficient and from Figures 8, 14 radiation patterns get altered due to the presence of head model.

The designed circular antenna gives overall good characteristics, but for small and portable handheld device the size will be too big, and SAR does not comply with IEEE, FCC, and ICNIRP guidelines and is higher than the values set by these standards [15–17]. To reduce SAR further and improve performance, investigation is required.

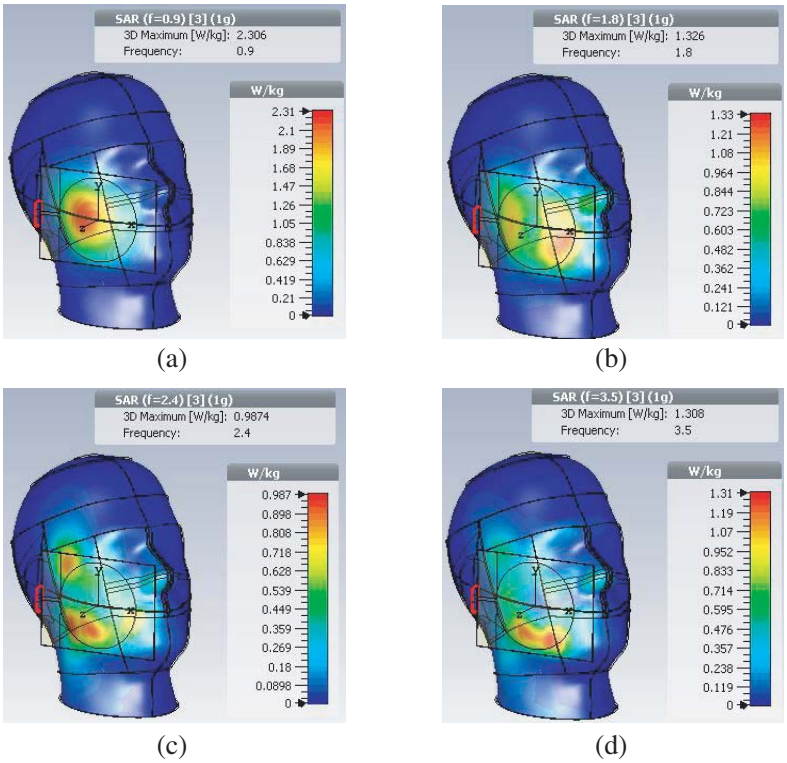

Figure 11. (a) to (d) SAR at 1-gram of tissue mass for circular antenna.

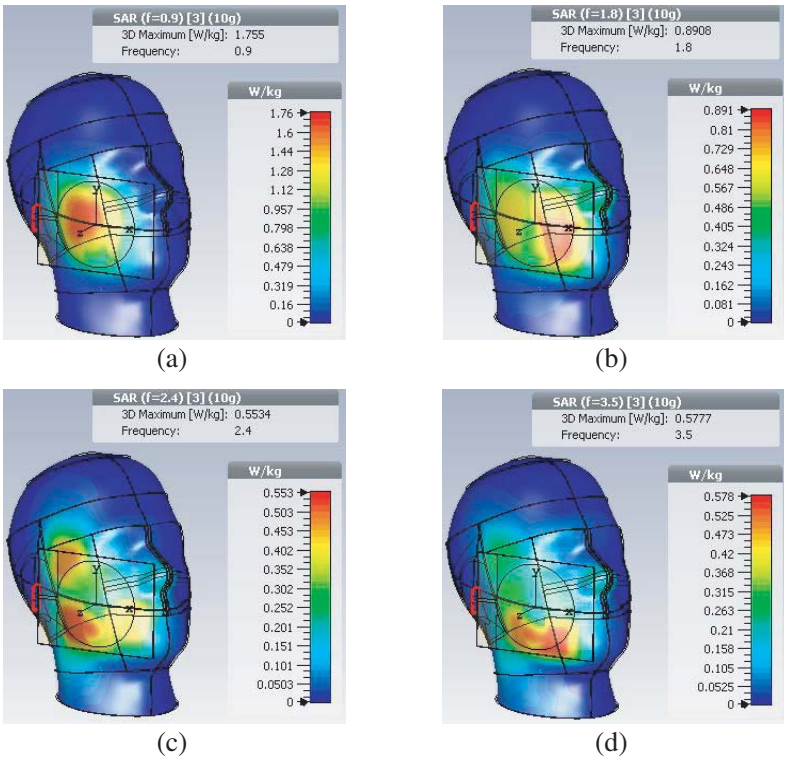

Figure 12. (a) to (d) SAR at 10-gram of tissue mass for circular antenna.

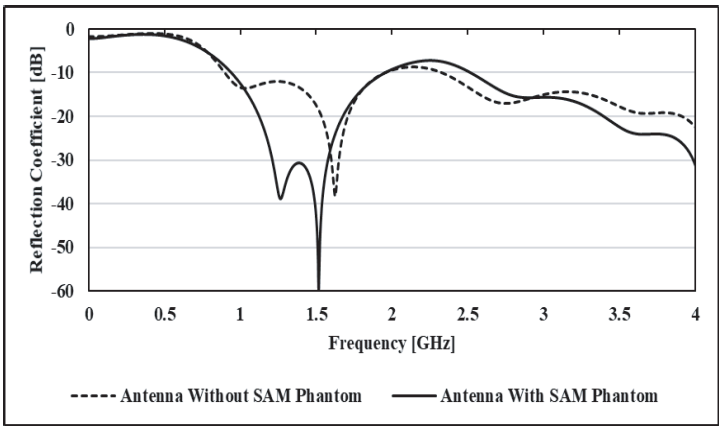

Figure 13. Variation in reflection coefficient v/s frequency for circular antenna.

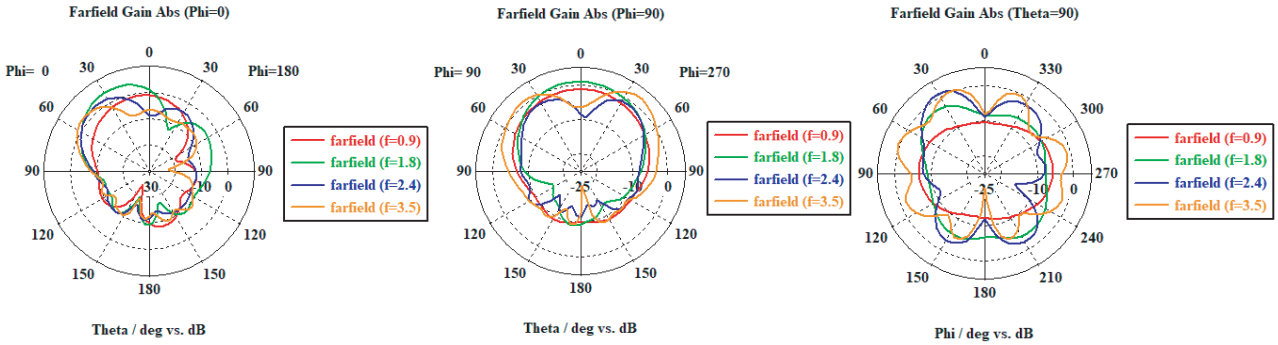

(a) (b) (c)

Figure 14. Simulated combined radiation pattern, (a) X-Z plane, (b) Y-Z plane, (c) X-Y plane.

2.2. Design of Annular Ring Antenna

The actual radius of concentric ring is '$(b-a)$' where b is the radius of outer ring and a is the radius of inner ring. Correction in radius is calculated using the first order approximation of Bessel function, and corrected radius is given by Equation (7) and is substituted in Equation (8) to get resonant frequency 'f_r' for the dominant mode TM_{11} [8].

$$(b-a)_e = (b-a)\left\{1+\frac{2h}{\pi(b-a)\varepsilon_r}\left[\ln\left(\frac{\pi(b-a)}{2h}\right)+1.7726\right]\right\}^{\frac{1}{2}} \tag{7}$$

$$f_r = \frac{1.8412c}{2\pi(b-a)_e\sqrt{\varepsilon_r}} \tag{8}$$

where h is the height of substrate, ε_r the relative dielectric constant, f_r the frequency of resonance, and $(b-a)_e$ the corrected radius.

The performance of annular ring antenna is optimized by varying the thickness of the ring, and usually the ratio of inner radius to the outer radius is varied in the range of 1.5 to 2 [5]. Figure 15 displays the design of an annular ring antenna having comparable dimensions with the circular antenna depicted in Figure 4.

Figure 16 depicts the variation in simulated reflection coefficient with respect to frequency when antenna is used with and without SAM phantom model with the same settings as discussed for Figure 13 above. It is witnessed that 2.4 GHz band is shifted upward, and reflection coefficient becomes greater than -10 dB. Figures 17(a) to (d) depict 3-D gain in dB, and Figures 18(a) to (d) show 3-D directivity

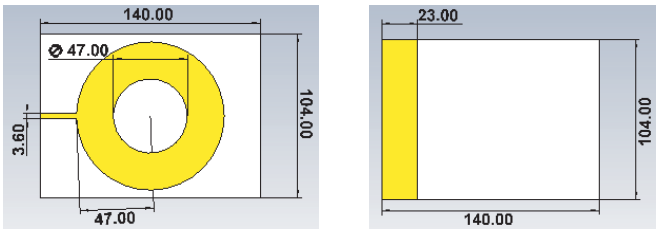

Figure 15. Top and bottom view of single feed annular ring antenna with partial ground.

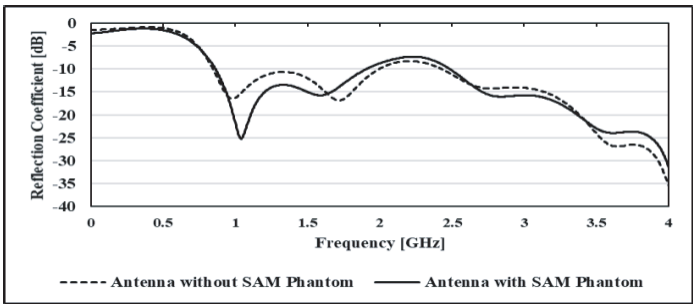

Figure 16. Variation in reflection coefficient of annular ring antenna with and without SAM phantom v/s frequency.

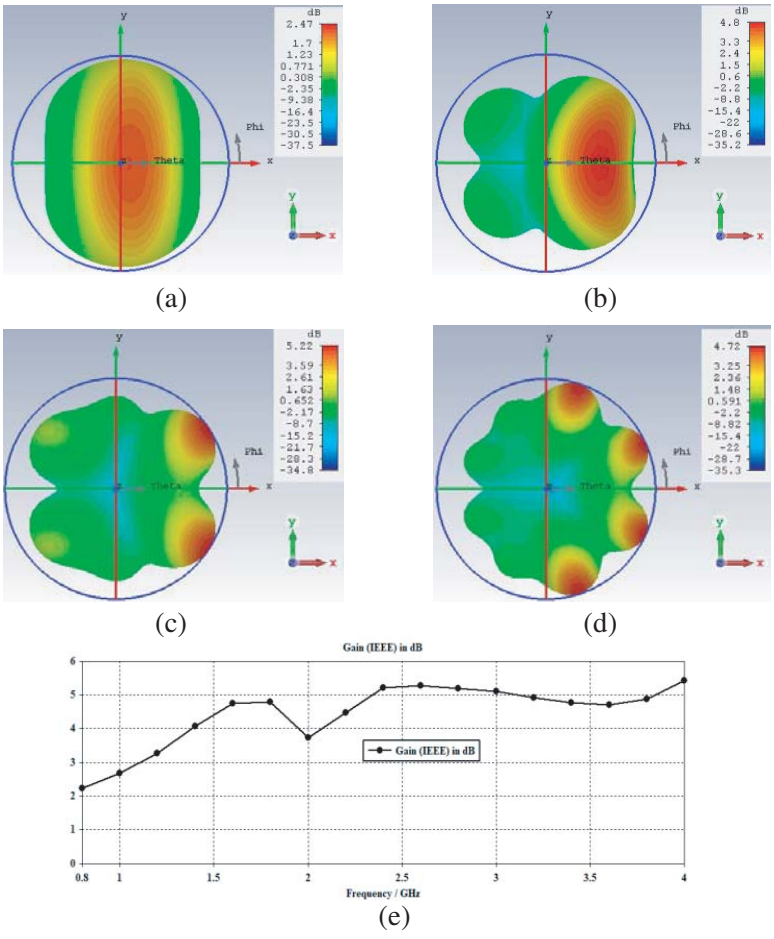

Figure 17. (a) to (d) Gain at desired frequencies, (e) gain v/s frequency over entire band.

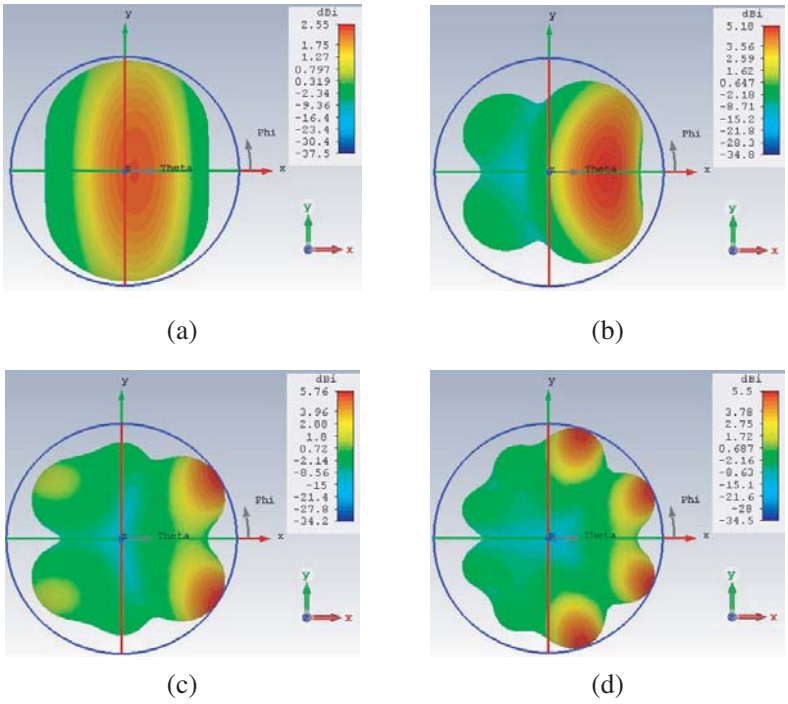

Figure 18. (a) to (d) Directivity in dBi at desired frequencies.

in dBi, at 0.9 GHz, 1.8 GHz, 2.4 GHz, and 3.5 GHz, respectively. Figure 17(e) shows the gain over the entire frequency band for annular ring antenna. It is apparent from the figures below that gain and directivity have slight variation for annular ring antenna compared with circular antenna. Radiation pattern, VSWR, and power curve are very much similar for circular and annular ring antennas.

Figures 19(a) to (d) depict simulated values of SAR for 1-gram tissue mass, and Figures 20(a) to (d) show at 10-gram tissue mass for frequencies of interest at 0.9 GHz, 1.8 GHz, 2.4 GHz, and 3.5 GHz, respectively.

2.3. Design of Dual Feed Annular Ring Antenna

A dual feed annular ring antenna is designed, and parametric study on size of circular slot in ground plane is performed for better return loss characteristics. Annular ring antenna and defect in ground plane is depicted in top and bottom views of Figure 21 and fabricated prototype in Figure 22. The single antenna element with two microstrip line feeds, symmetrical on both sides, is used to enhance gain and reduce SAR, and circular slot in ground is made and assessed for the variation of radius from 10 mm to 45 mm to optimize the performance of antenna. When the size of the circular slot in ground overlaps with the outer ring of annular ring patch, it influences the change in surface current, and the wideband performance of antenna is obtained. Also, outer to inner ring radius ratio is varied from 2 to 3, and this variation causes further improvement in the performance of dual feed annular ring. It is witnessed that the enhancement happens in terms of matching the impedance, gain, and bandwidth along with reduction in the volume of antenna. To achieve the reduction in SAR while maintaining other performance parameters of antenna, a novel technique of dual feeds on opposite sides is used with half input power and out of phase excitation so gain and directivity are added constructively whereas volume of antenna and losses are reduced which is discussed in results section.

2.3.1. Ideal Transformer Method

The dual feed annular ring with circular DGS in ground plane can be characterized using ideal transformer model method, and turns ratio in windings indicates the number of circular slots. Single

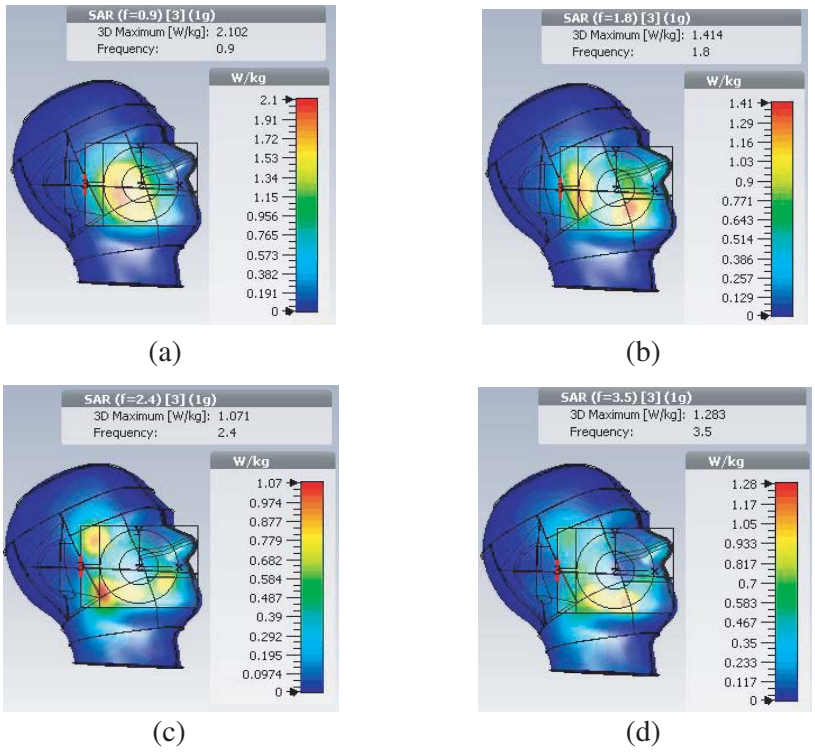

Figure 19. SAR at 1-gram of tissue mass for annular ring antenna.

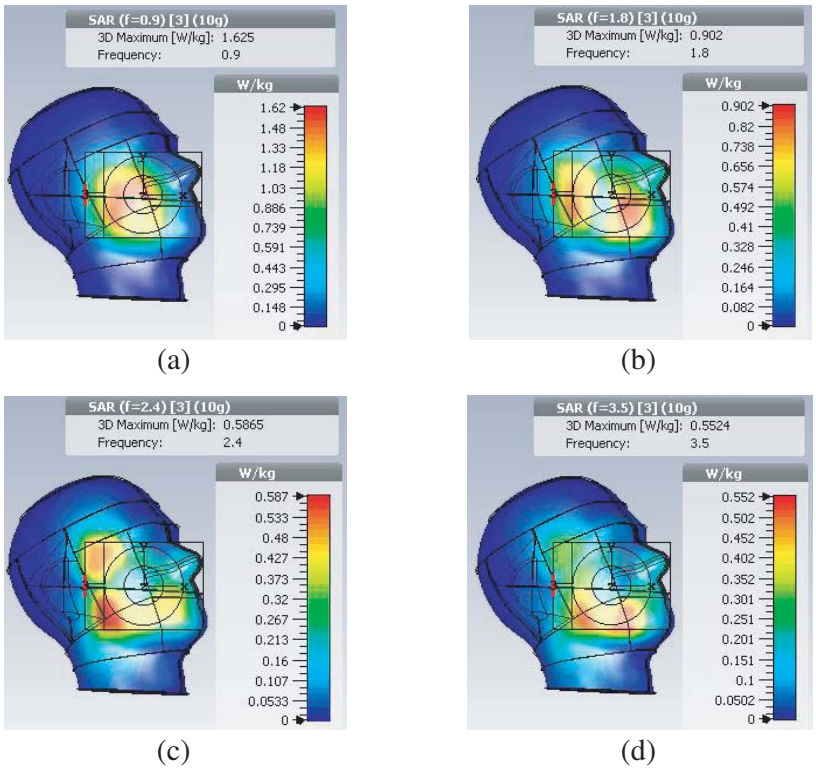

Figure 20. (a) to (d) SAR at 10-gram of tissue mass for annular ring antenna.

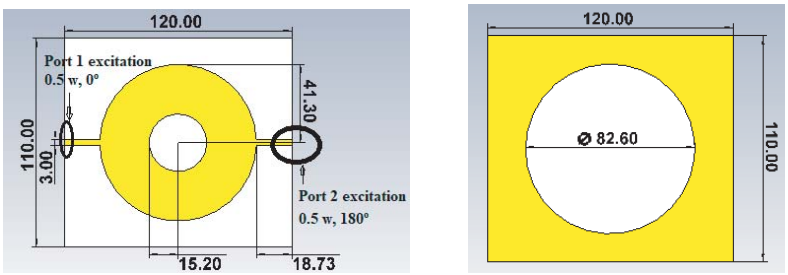

Figure 21. Top view and bottom view of proposed designed dual feed annular ring antenna.

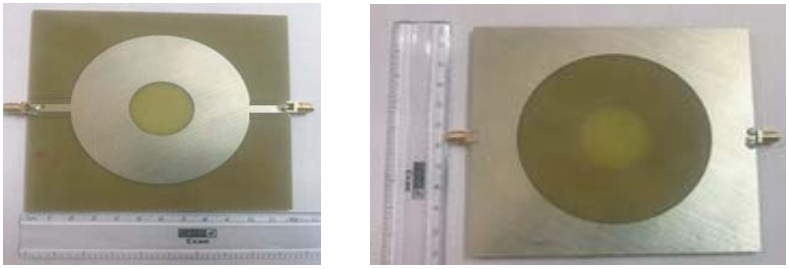

Figure 22. Top view and bottom view of fabricated proposed dual feed annular ring antenna.

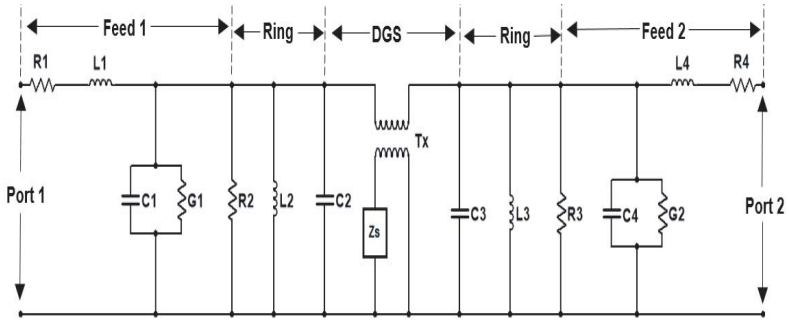

Figure 23. Equivalent circuit model of dual feed annular ring antenna with DGS.

slot is used underneath the patch, so primary and secondary windings have equal turns, and the ratio corresponds to 1. An ideal transformer is used to indicate the coupling between annular ring antenna and circular slot in ground. The slot is represented by characteristic impedance Z_S. Distributed elements represent microstrip feeds, and RLC parallel tuned circuit represents the annular ring [13]. Equivalent circuit model is shown in Figure 23.

2.3.2. Parametric Study on Defect in Ground Plane

Figures 24(a) and (b) present variation curves of reflection coefficient with respect to frequency, and circular slot is made in the ground plane varying from size of 10 mm in a step of 5 mm each.

It is observed that due to the defect in ground plane, multiple bands are obtained, and the optimization in defect size is required to get desired bands. When the size of DGS varies between 10 mm and 30 mm, bandwidth achieved for multiple bands is narrow. Besides, whenever defect size varies from 30 mm to 40 mm, bandwidth is broadened for multiple bands. Further increase in the size of the circular slot in ground plane from 40 mm to 45 mm, it is witnessed that suddenly reflection coefficient value increases, and all the desired bands vanish due to poor impedance matching. When the size of DGS is 40 mm, the value of reflection coefficient is less than -10 dB for all the bands of

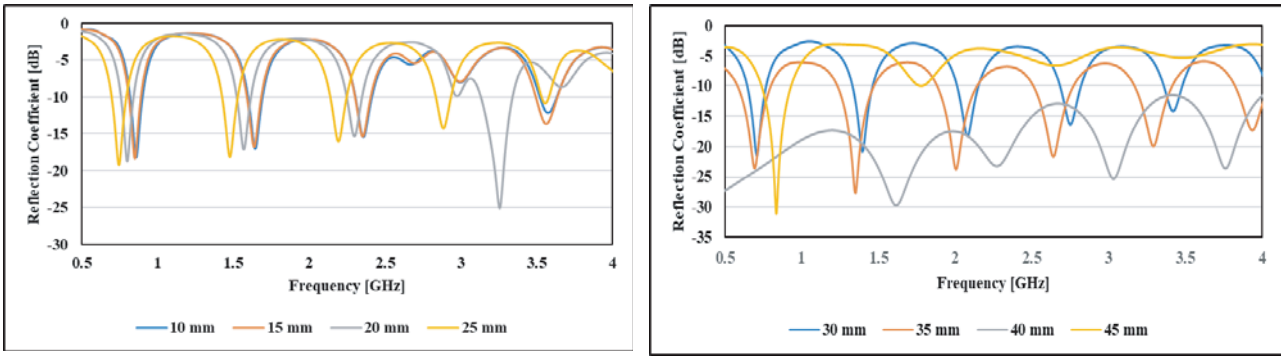

(a) (b)

Figure 24. (a) and (b) Reflection coefficient v/s frequency for different sizes of DGS.

interest, and the performance of antenna appears to be wideband, but by analysing the increasing trend of reflection coefficient it is predicted that the higher bands will diminish above 5 GHz. So further optimization of DGS is required on minor scale between 40 mm and 42 mm. After further investigation, the optimum size found for circular slot in ground is 41.3 mm, where all the desired bands required for mobile communication with enhanced gain are achieved, and the antenna behaves as a wideband antenna.

3. RESULTS AND DISCUSSION

3.1. Reflection Coefficient

Simulated and measured reflection coefficients are presented in Figure 25 for dual feed annular ring antenna at four resonant frequencies, and as ports are symmetrical, individual ports are excited, and measurements are carried out. The result presented below is for port 1 being excited and port 2 terminated with a 50 Ω impedance terminator. From the result it is evident that simulated and measured S_{11} are below −10 dB for all the desired bands. The measured S_{11} at the first band (850/900 MHz) is −28.88 dB at resonant frequency of 852 MHz, and impedance bandwidth obtained is 413 MHz (0.587–1 GHz). For the second band (1800/1900 MHz) it gives −20.30 dB at 1.857 GHz frequency of resonance, and impedance bandwidth achieved is 470 MHz (1.630–2.100 GHz). For third band (2.4 GHz), it is

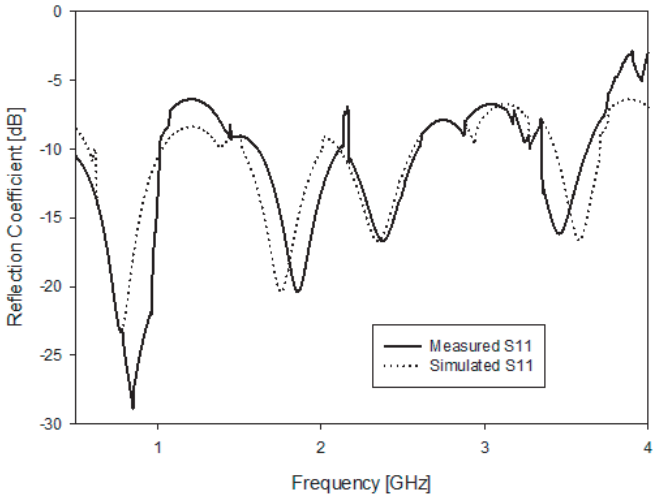

Figure 25. Simulated and measured reflection coefficient v/s frequency at port 1.

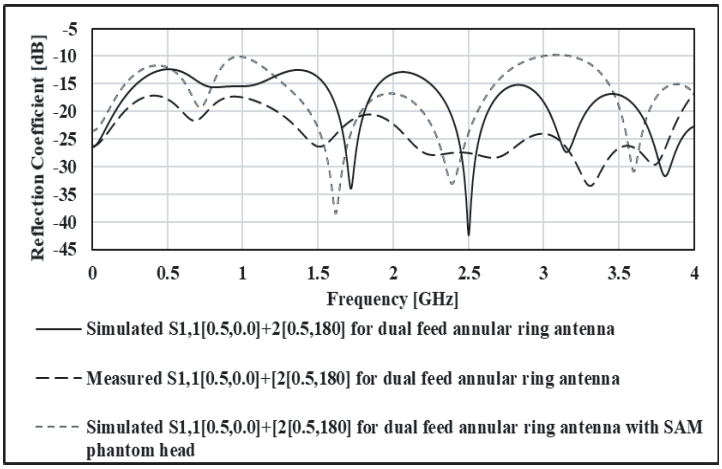

Figure 26. Simulated and measured reflection coefficient v/s frequency for port 1 and 2 when simultaneously excited and simulated reflection coefficient when antenna is aligned with SAM phantom model.

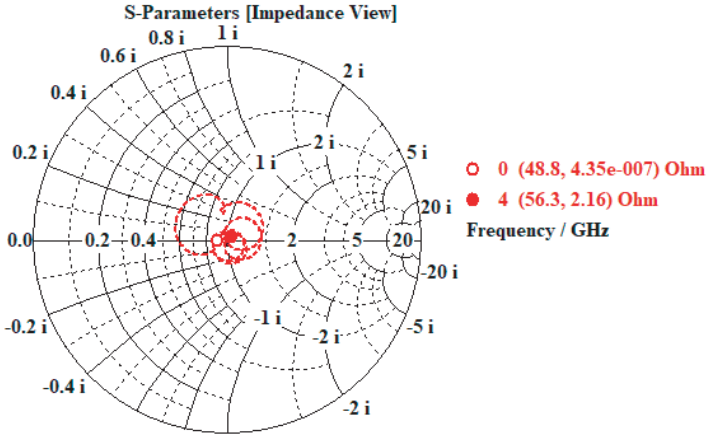

Figure 27. Simulated impedance variation of antenna with simultaneous excitation (Smith Chart).

−16.63 dB at the resonance frequency of 2.38 GHz, and impedance bandwidth is 439 MHz (2.171–2.610 GHz). The fourth band (3.5 GHz) gives S_{11} as −16.10 dB at the resonant frequency of 3.45 GHz, and the bandwidth is 261 MHz (3.357–3.618 GHz).

Figure 26 illustrates simulated and measured reflection coefficients for dual feed annular ring antenna. Port 1 is excited through 0.25 W simulated power input with 0° phase, and port 2 is excited with 0.25 W simulated power input with 180° phase. It is witnessed that the widening of bands occurs, and multiband antenna performance changes to wideband. Reflection coefficient is less than −10 dB from 0 to 4 GHz. Simulated results for reflection coefficient of antenna in the presence of SAM phantom model are also compared with simulated and measured results of reflection coefficients of the prototype without head model in single graph, and slight deviation is noticed. Results are in good agreement, and the deviation in measured and simulated results may be due to accuracy in fabrication and simultaneous measurement. Figure 27 shows simulated result of impedance variation of antenna when both the ports are simultaneously fed using the above mentioned method.

3.2. Gain and Directivity of Dual Feed Annular Ring Antenna at Different Bands

Figures 28(a) to (d) and Figures 29(a) to (d) show 3D-Gain and 3D-Directivity, respectively. For the first band at 0.9 GHz, gain is 2.98 dB, and directivity is 3.27 dBi. For the second band at 1.8 GHz, gain

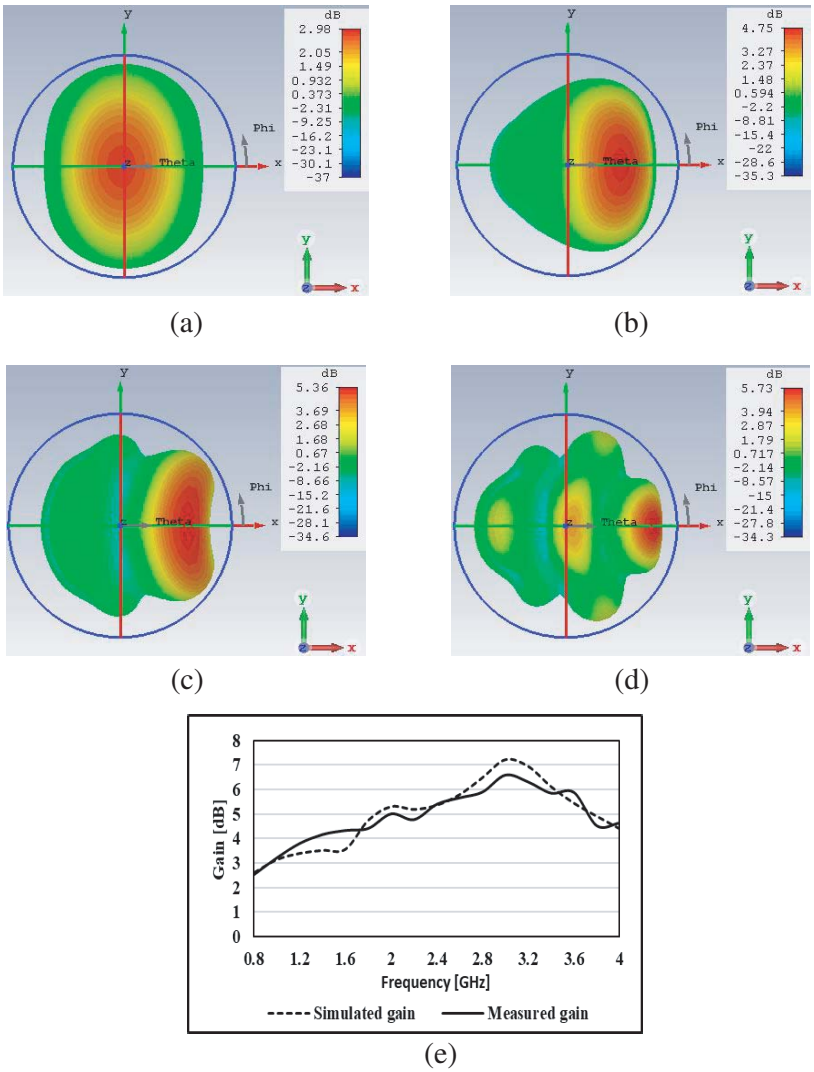

Figure 28. (a) to (d) Gain at desired frequency, (e) gain v/s frequency over entire band.

is 4.75 dB, and directivity is 5.44 dBi. For the third band at 2.4 GHz, gain is 5.36 dB, and directivity is 5.99 dBi. For the fourth band at 3.5 GHz, gain is 5.73 dB, and directivity is 6.76 dBi. Figure 28(e) shows simulated and measured values of gain plotted over the entire band of frequency. From values of gain and directivity, it is evident that as frequency increases, the values of gain and directivity are increased, and generally radiation efficiency is also increased.

3.3. Radiation Patterns for Different Bands

Figures 30(a) to (c) show simulated combined radiation patterns at 0.9 GHz, 1.8 GHz, 2.4 GHz, and 3.5 GHz in X-Z plane, Y-Z plane, and X-Y plane, respectively. Radiation pattern figure looks like donut shape at 0.9 GHz, 1.8 GHz, and the number of lobes will rise with the increase in frequency. Over-The-Air (OTA) test is performed for radiation pattern and range measurement using walkie talkie programmable handsets operating over wide range covering all the bands from (400 MHz to 4.5 GHz), and the method and setup are discussed in detail in [18] and used to carry out measurements. Figure 31(a) depicts walkie talkie handset with helical antenna and another handset with the proposed antenna. User 1 is handling walkie talkie 1 and is stationary on the roof of building, whereas user 2 is handling walkie talkie 2 and is a moveable user communicating with user 1. Figure 31(b) depicts GPS locating

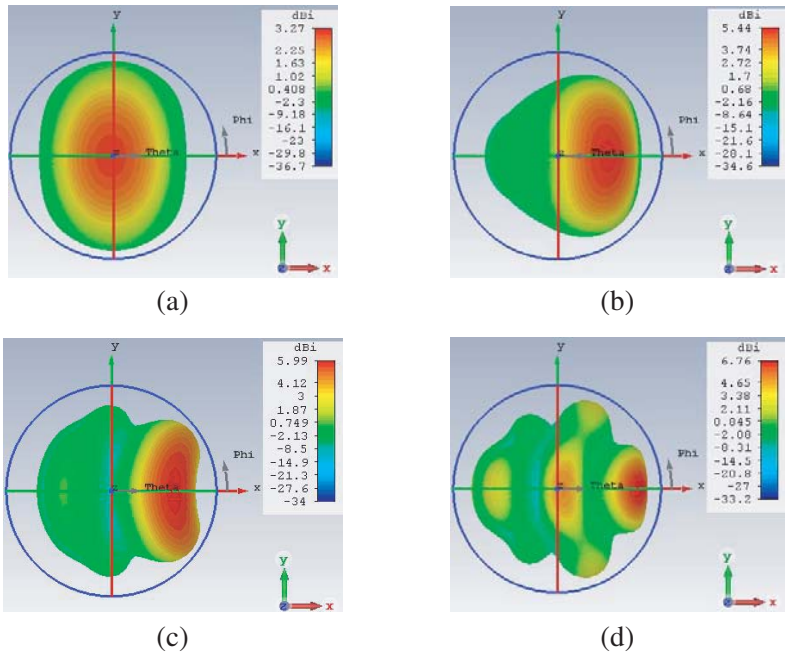

Figure 29. (a) to (d) Directivity in dBi at desired frequency.

devices, and locations are marked with MapSource Tool which will locate user 2 with reference to user 1, plot the pattern at some discrete points, and also measure the distance of user 2 from user 1. Figure 31(c) shows the plot from MapSource Tool indicating the pattern and distance covered in OTA test, given in Table 1.

Table 1. Outdoor measurement.

Angle [degrees]	Distance covered [meters]	Position of antenna
0	246	Broad side 3
14	472	Broad side 4
24	802	End of null 1
50	1010	End of null 2
56	1010	Broad side 7
70	968	Broad side 8
101	543	Broad side 9
115	292	Broad side 6
165	487	Broad side 5
206	710	Null 3
213	1010	End of null 3
238	157	Null 2
282	95	Null 1
306	84	Broad side 1
324	96	Broad side 2

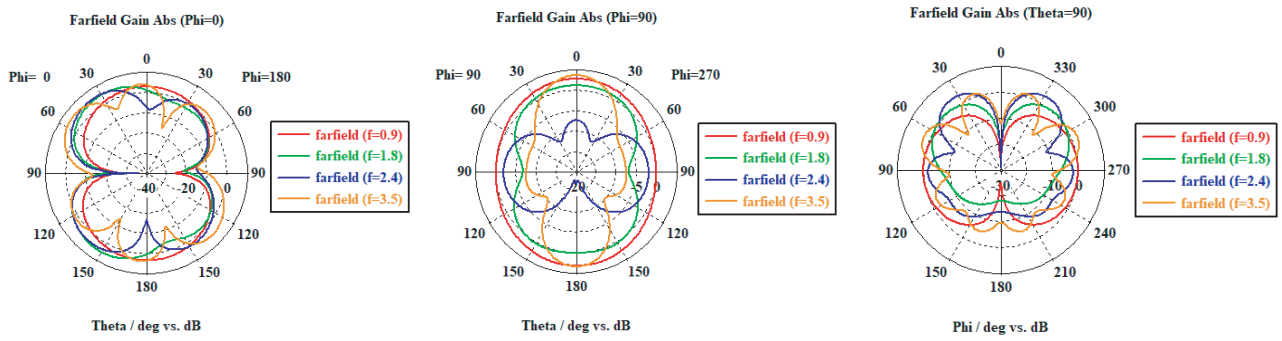

(a) (b) (c)

Figure 30. Simulated radiation pattern, (a) X-Z plane, (b) Y-Z plane, (c) X-Y plane.

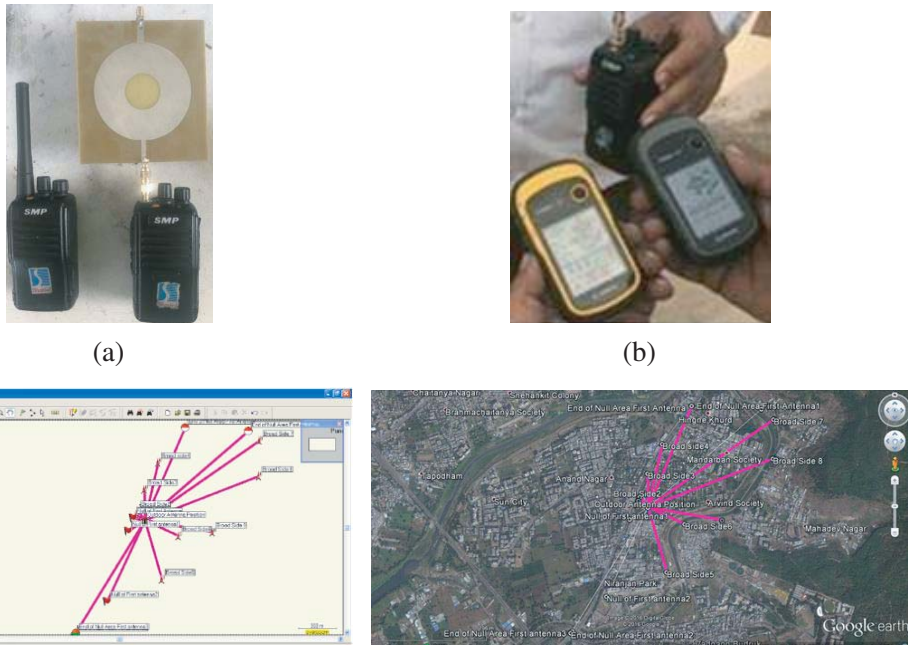

(a) (b)

(c) (d)

Figure 31. (a) and (b) Test equipment's, (c) measurement of range and radiation pattern using OTA test, (d) mapping with google earth.

3.4. Power Curve

Figures 32(a) and (b) depict distributed powers simulated at port 1 and port 2 when they are excited independently along with the losses incurred in metallic patch and dielectric substrate, and low loss tangent substrate will reduce losses. Also efficient design with better impedance matching will radiate more accepted power from input power applied. The losses incurred in metal and substrate are comparatively less in dual feed annular ring antenna with circular DGS than circular antenna and single feed annular ring antenna with partial ground, and are evident from Figure 10 and Figure 32.

3.5. SAR at Different Frequencies

Figures 33(a) to (d) give values of SAR in W/Kg in mass of 1-gram of tissue at all desired frequencies when port 1 is excited with 0.5 W input power and 0° phase, and port 2 is excited with 0.5 W input

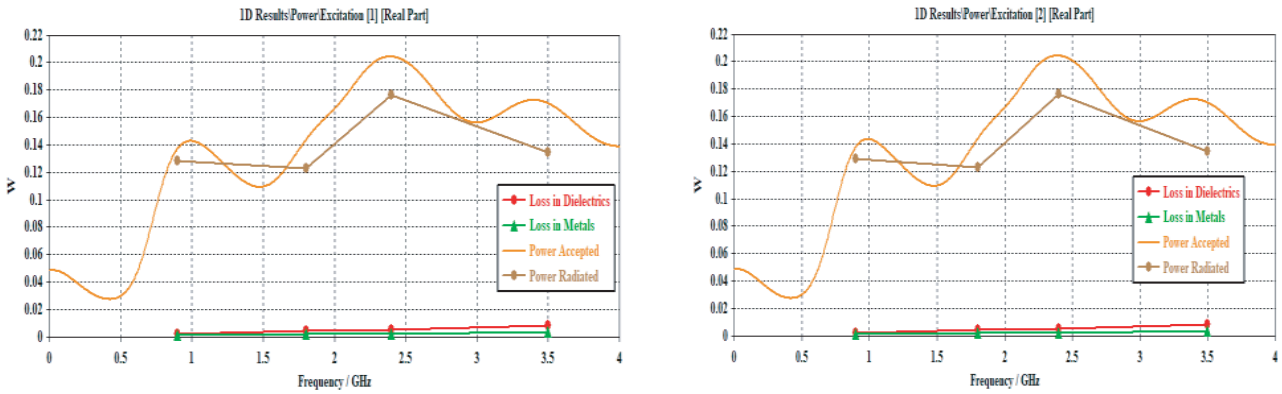

(a) (b)

Figure 32. Power and losses curves at (a) port 1 and (b) port 2.

Table 2. Comparison of SAR for designed antennas.

Frequency [GHz]	Circular antenna [W/Kg]		Annular ring antenna [W/Kg]		Dual feed annular ring antenna [W/Kg]	
	1 g	10 g	1 g	10 g	1 g	10 g
0.9	2.306	1.755	2.102	1.625	0.695	0.578
1.8	1.326	0.8908	1.414	0.902	0.311	0.189
2.4	0.987	0.553	1.071	0.5865	0.218	0.12
3.5	1.308	0.5777	1.283	0.5524	0.229	0.0989

Table 3. Comparison of SAR [W/Kg] v/s frequency [GHz].

Reference No. and Year	0.9		1.8		2.4		3.5	
	1 g	10 g	1 g	10 g	1 g	10 g	1 g	10 g
[19], 2017	-	-	1.16	0.88	0.484	0.18	1.01	0.799
[20], 2017	-	-	-	-	1.31	-	-	-
[21], 2015	2.25	1.5	-	1.53	-	-	-	-
[22], 2014	-	0.84	-	0.80	-		-	-
[23], 2014	-	0.93	-	0.80	-		-	-
[24], 2010	1.14	-	0.62	-	0.26	-	-	-
[25], 2010	2.119	-	2.137	-	-	-	-	-
[26], 2009	2.02	1.39	1.06	0.58	-	-	-	-
[27], 2009	1.5	0.52	2.64	0.85	-	-	-	-
proposed	0.695	0.578	0.311	0.189	0.218	0.12	0.229	0.099

power and 180° phase. SAR evaluated is for simultaneously applied inputs at both the ports. SAR at 0.9 GHz band is 0.695 W/kg, at 1.8 GHz band is 0.311 W/Kg, at 2.4 GHz band is 0.218 W/Kg, and at 3.5 GHz band is 0.229 W/Kg. Figures 34(a) to (d) give values of SAR in W/Kg in mass of 10-gram of tissue at all desired frequencies. Evaluated values for SAR revealed use simultaneous excitation at port 1 and port 2 at 10 g. SAR at 0.9 GHz band is 0.578 W/Kg, at 1.8 GHz band is 0.189 W/Kg, at 2.4 GHz

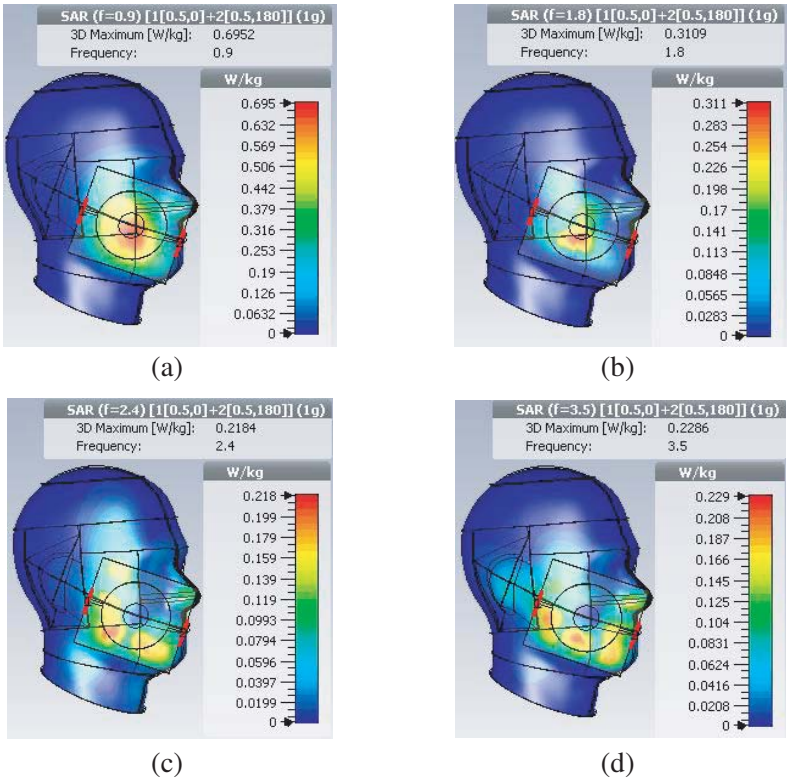

Figure 33. (a) to (d) SAR at 1-gram for dual feed annular ring antenna with simultaneous excitation.

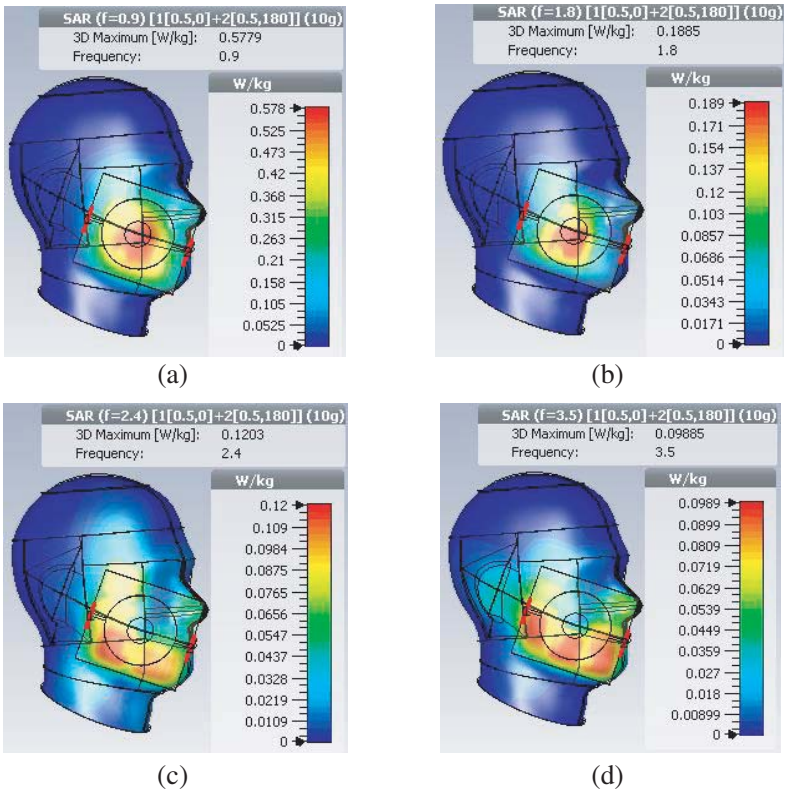

Figure 34. (a) to (d) SAR at 10-gram for dual feed annular ring antenna with simultaneous excitation.

band is 0.12 W/Kg, and at 3.5 GHz band is 0.0989 W/Kg. All values of SAR for three different antenna configurations are compared in Table 2. It is evident that SAR is reduced drastically for all desired frequencies when applied inputs are out of phase by 180°. All the values of SAR obtained for dual feed annular ring antenna with circular DGS are very much below 1.6 W/Kg in 1-gram tissue mass as per the guidelines of FCC and IEEE and 2 W/Kg in 10-gram tissue mass as per ICNIRP standard. The major focus of reducing SAR succeeds at 0.9 GHz and 1.8 GHz as these frequencies are used in calling mode, whereas 2.4 GHz and 3.5 GHz bands are used for Wi-Fi/Bluetooth and WiMAX, where generally handheld gadgets are kept away from head and body. Table 3 gives comparison with existing work.

4. CONCLUSIONS

Annular ring antenna size is comparatively less than circular antenna for same resonant frequency. The multiband operation of antennas can be achieved using defect in ground plane (DGS), and circular defect produces wideband operation. Instead of using multiple single band antennas, multiband or wideband antenna can be used which will reduce the overall cost of product. Outer to inner ring radius ratio is varied in range between 2 and 3, and it is noticed that the gain for lower frequency band of operation is higher, if the ratio is close to 3, and the gain for higher band of operation is higher if the ratio is close to 2, so it is always a negotiation to have a suitable ratio to get optimum performance in all desired bands, and ratio utilized is 2.72. When each port of dual feed annular ring is excited separately with half input power and 180° out of phase, it produces less SAR than single feed circular antenna, and in dual feed annular ring antenna the volume of of antenna is reduced by 9.3%, and gain and directivity are enhanced by 9% and 14.79%, respectively. Surface waves and dielectric losses are reduced by more than 50% due to the circular DGS underneath annular ring in ground and conducting material removed, and consequently SAR is reduced up to 82.15%.

ACKNOWLEDGMENT

Authors would like to thank Mr. Anirudhda Kulkarni, Cyronics Instruments Pvt. Ltd. Pune, India and Mr. Mukund Bhople for providing help and support while carrying out OTA test.

REFERENCES

1. Campbell, D. and C. J. Reddy, "Antenna design considerations for LTE enabled tablets," *IEEE International Symposium on Antennas and Propagation & USNC/URSI National Radio Science Meeting*, 1140–1141, Vancouver, 2015.
2. Wong, K., "4G/Multiband handheld device ground antennas," *Asia-Pacific Microwave Conference Proceedings (APMC)*, 134–136, Seoul, 2013.
3. Gampala, G., C. J. Reddy, O. Stabler, and T. Hager, "Compact antenna for MIMO LTE mobile phone applications," *Microwave Journal*, Vol. 55, No. 3, 98–110, 2012.
4. Chew, W., "A broad-band annular-ring microstrip antenna," *IEEE Transactions on Antennas and Propagation*, Vol. 30, No. 5, 918–922, Sept. 1982.
5. El-khamy, S., R. El-Awadi, and E. A. El-Sharrawy, "Simple analysis and design of annular ring microstrip antennas," *IEE Proceedings H — Microwaves, Antennas and Propagation*, Vol. 133, No. 3, 198–202, 1986.
6. Chakraborty, S. and S. Srivastava, "High gain annular ring antenna," *International Conference on Devices and Communications (ICDeCom)*, 1–5, Mesra, 2011.
7. Garg, R., *Microstrip Antenna Design Handbook*, Artech House, Boston, 2001.
8. Balanis, C., *Antenna Theory: Analysis and Design*, Reprint, Wiley, New-Delhi, India, 2016.
9. Guha, D., M. Biswas, M. Yahia, and M. Antar, "Microstrip patch antenna with defected ground structure for cross polarization suppression," *IEEE Antennas and Wireless Propagation Letters*, Vol. 4, 455–458, 2005.

10. Caloz, C., H. Okabe, T. Iwai, and T. Itoh, "A simple and accurate model for microstrip structures with slotted ground plane," *IEEE Microwave and Wireless Components Letters*, Vol. 14, No. 4, 133–135, Apr. 2004.
11. Lin, D.-B., I.-T. Tang, and M.-Z. Hong, "A compact quad-band PIFA by tuning the defected ground structure for mobile phones," *Progress In Electromagnetics Research B*, Vol. 24, 173–189, 2010.
12. Chen, Z., Y.-L. Ban, J.-H. Chen, J. L.-W. Li, and Y.-J. Wu, "Bandwidth enhancement of LTE/WWAN printed mobile phone antenna using slotted ground structure," *Progress In Electromagnetics Research*, Vol. 129, 469–483, 2012.
13. Khandelwal, M., B. Kanaujia, and S. Kumar, "Defected ground structure: Fundamentals, analysis, and applications in modern wireless trends," *International Journal of Antennas and Propagation*, 1–22, 2017.
14. Lin, J. C., "Specific absorption rates (SARs) induced in head tissues by microwave radiation from cell phones," *IEEE Antennas and Propagation Magazine*, Vol. 42, No. 5, 138–139, Oct. 2000.
15. Institute of Electrical and Electronic Engineers (IEEE), IEEE C95.1-2005, *Standards for Safety Levels with Respect to Human Exposure to Radio Frequency Electromagnetic Fields*, IEEE Press, New York, 2005.
16. US Federal Communication Commission, Office of Engineering and Technology, "Evaluating compliance with FCC-specified guidelines for human exposure to radio radiofrequency radiation," OET Bulletin 65, Washington, DC, 1997.
17. International commission on Non-Ionizing Radiation Protection (ICNIRP), "Guidelines for limiting exposure to time-varying electric, magnetic, and electromagnetic fields (up to 300 GHz)," *Health Physics*, Vol. 74, 494–522, 1998.
18. Munde, M., A. Nandgaonkar, and S. Deosarkar, "Low specific absorption rate antenna using electromagnetic band gap structure for long term evolution band 3 application," *Progress In Electromagnetics Research M*, Vol. 80, 23–34, 2019.
19. Agrawal, T. and S. Srivastava, "Compact MIMO antenna for multiband mobile applications," *Journal of Microwaves, Optoelectronics and Electromagnetic Applications*, Vol. 16, No. 2, 542–552, 2017.
20. Bhattacharjee, S., M. Mitra, and S. R. Bhadra Chaudhuri, "An effective SAR reduction technique of a compact meander line antenna for wearable applications," *Progress In Electromagnetics Research M*, Vol. 55, 143–152, 2017.
21. Faruque, M., M. Hossain, and M. Islam, "Low specific absorption rate microstrip patch antenna for cellular phone applications," *IET Microwaves, Antennas & Propagation*, Vol. 9, No. 14, 1540–1546, Nov. 2015.
22. Abdullah, H. H. and K. S. Sultan, "Multiband compact low sar mobile hand held antenna," *Progress In Electromagnetics Research Letters*, Vol. 49, 65–71, 2014.
23. Sultan, K., H. Abdullah, and E. Abdallah, "Low SAR, simple printed compact multiband antenna for mobile and wireless communication applications," *International Journal of Antennas and Propagation*, Vol. 2014, 1–8, 2014.
24. Wong, K., W. Chen, C. Wu, and W. Li, "Small-size internal eight-band LTE/WWAN mobile phone antenna with internal distributed LC matching circuit," *Microwave Optical Technology Letters*, Vol. 52, 2244–2250, 2010.
25. Chiu, C.-W., C.-H. Chang, and Y.-J. Chi, "Multiband folded loop antenna for smart phones," *Progress In Electromagnetics Research*, Vol. 102, 213–226, 2010.
26. Cabedo, A., J. Anguera, C. Picher, M. Ribo, and C. Puente, "Multiband handset antenna combining a PIFA, slots, and ground plane modes," *IEEE Transactions on Antennas and Propagation*, Vol. 57, No. 9, 2526–2533, Sept. 2009.
27. Kang, T. and K. Wong, "Chip-inductor-embedded small-size printed strip monopole for WWAN operation in the mobile phone," *Microwave Optical Technology Letters*, Vol. 51, 966–971, 2009.